Extending the applications of a stacked X-ray detector system to a Compton camera

Bachelorarbeit
der Mathematisch-Naturwissenschaftlichen Fakultät
am Institut für Astronomie und Astrophysik
der Eberhard Karls Universität Tübingen
zur Erlangung des akademischen Grades
Bachelor of Science (B. Sc.)

vorgelegt von
Matthias Biegger

Tübingen
November 2016

Hiermit versichere ich, Matthias Biegger, Matrikelnummer 3774265, dass ich gemäß des allgemeinen Teils der Studien- und Prüfungsordnung der Universität Tübingen für den Studiengang Physik mit akademischer Abschlussprüfung Bachelor of Science (B. Sc.) vom 30.07.2013 diese Bachelorarbeit mit dem Titel

Extending the applications of a stacked X-ray detector system to a Compton camera

selbstständig und keine anderen als die angegebenen Hilfsmittel und Quellen benutzt habe. Außerdem versichere ich, dass alle wörtlich oder sinngemäß aus anderen Werken übernommene Aussagen als solche gekennzeichnet habe und dass die Arbeit weder vollständig noch in wesentlichen Teilen Gegenstand eines anderen Prüfungsverfahrens gewesen ist. Die Arbeit ist weder vollständig noch in wesentlichen Teilen bereits veröffentlicht worden. Das in Dateiform eingereichte Exemplar stimmt mit den eingereichten gebundenen Exemplaren überein.

Ort, Datum	Unterschrift

Abstract

This work is based on a stacked X-ray detector system which contains a low energy detector made of silicon and a high energy detector made of cadmium telluride with a very high quantum efficiency (close to 100 %) between 0.1 keV and 100 keV.

A live software named CASIMEO is presented in the first part of this thesis which displays the transmitted data of the detectors during a measurement. It is able to visualize up to four plots for each detector: a hitmap, a hitrate in units per frame, a hitrate in units per time and a spectrum of the pulse height amplitude of the events. The results of CASIMEO are illustrated by two measurements. The first one was done with a special mask to show the spatial resolution of the low energy detector. The second measurement with a duration of about 25 ks was executed with an americium source without any mask.

The aim of the second part is to analyse Compton scattering events to trace back the position of an X-ray source in three dimensions. Therefore, the data of both detectors of one measurement have to be preprocessed and filtered first. The remaining events coming from Compton scattering processes can be used to illustrate with ellipses the directions where the initial photons could have come from. The superposition of those ellipses which indicates the position of the X-ray source marks the result of the analysis followed by a discussion of those results. Since the reconstruction of the source position does not match the real location of the source, the properties of the detector setup have still to be improved for an application as a Compton camera.

Contents

Chapter 1

Introduction

Astronomers carry out observations of the universe to explore and understand its complexity. It is common to observe many different kinds of information coming from a source. This includes messengers like photons, particles or gravitational waves, but also their attributes such as the direction, intensity, energy or polarization of radiation. For photons, observations are performed by using telescopes and detectors which are designed for the respective energy band. As shown in Figure 1.1, the atmosphere of the Earth absorbs photons depending on their energy, whereby the absorption is strongest in the UV and X-ray band. That is why astronomers can use earthbound telescopes for radio waves and visible light. But for the majority of the electromagnetic spectrum it is common to observe above the atmosphere, with instruments located for example on satellites.

1.1 X-ray astronomy

In X-ray astronomy, photons with an energy between approximately 0.1 keV and 100 keV are the observed messengers. However, those energy limits are not clearly defined and vary in literature. At those energies, an observation from the surface of the Earth is not possible (see Figure 1.1), so today it is common to use instruments mounted on satellites for an observation. But building a space telescope is not possible without difficulties, for example the limited size and weight which are given by the launch vehicle. Another problem is that single components of the telescope can not be repaired or exchanged as soon as it has been launched. The last fact also limits the lifetime of the telescope until an essential component of the telescope is not working anymore or consumables for the thrusters are used up.

In X-ray astronomy observations are characterized by very low source fluxes. Because of that, an X-ray telescope should have a very high detection efficiciency. Instrument designers aim for a light telescope with a large

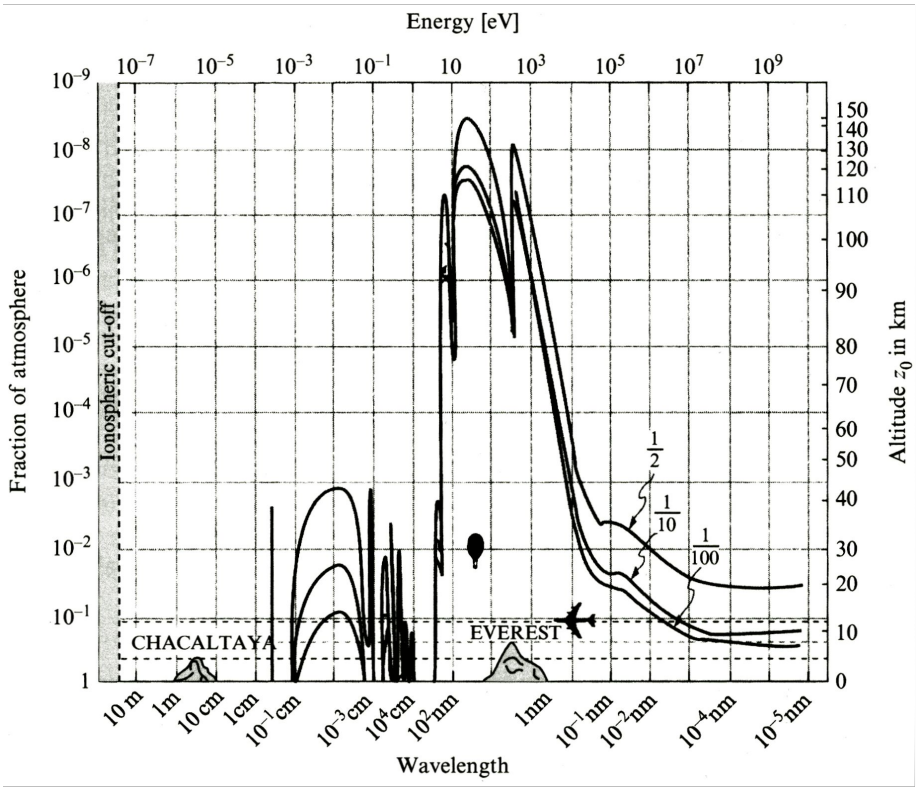

Figure 1.1: The absorption of electromagnetic waves in the atmosphere of the Earth is shown in dependence on the energy of the photons. There is an optical and a radio "window" which means the sky can be observed with telescopes from the surface of the Earth. For the other energies it is common to use telescopes in space. Image: Léna et al. (2012)

collecting area to minimize the observation time for a single source. Two well known X-ray satellites observing currently (2016) are *XMM-Newton* (Jansen et al., 2001) and *Chandra* (Weisskopf et al., 2002). Both of them use Wolter telescopes which consist of many mirror shells to reflect the X-ray photons under small incident angles to a focal plane where they will be detected. Both satellites carry several instruments where each of them often has its focus on one of the following parameters: angle-, energy- or time resolution, depending on its scientific purpose.

In recent years there is a trend to realize stacked detector systems to enlarge energy bands of X-ray observations. Such a detector system made of a low energy detector (LED) and a high energy detector (HED) was developed at the Institute of Astronomy and Astrophysics Tübingen (Maier, 2015). The work presented in the next chapters is based on this detector setup with the purpose to analyze Compton scattering events and trace

them back to the source they came from. This extends the scientific capabilities of such an instrument by providing applications as a Compton camera and Compton polarimeter. The part of the Compton camera is the core of this work and is explained in detail in Chapter 3. As a preparation for the data analysis of the camera, a near-realtime analysis software for the incoming events of both detectors was implemented and will be presented in Chapter 2. Before the main work of this thesis will be presented, a short introduction to the detector setup is given in the following Section 1.2.

1.2 The CANDELA setup

The CANDELA (**ca**dmium telluride and silico**n** **de**tector **la**boratory) is a stacked setup of a low energy detector (LED) and a high energy detector (HED) developed at the Institute of Astronomy and Astrophysics Tübingen (IAAT). Most of the information in this section are taken from the doctoral thesis of Maier (2015). The detectors are two independent systems which can be run alone as well as in a common operation mode. The setup contains radioactive sources to realize defined photon energies and counting rates. There are a ${}^{55}_{26}\mathrm{Fe}$ and two ${}^{241}_{95}\mathrm{Am}$ sources with an activity of $A_{\mathrm{Fe}} = 5.59\,\mathrm{MBq}$, $A^1_{\mathrm{Am}} = 1.66\,\mathrm{kBq}$ and $A^2_{\mathrm{Am}} = 2.82\,\mathrm{MBq}$ with reference of the values to the year 2015. A mechanical shutter allows to switch between the sources or block the emitted X-rays. Additionally, there are materials (aluminium, titanium and copper) emitting fluorescence lines when a source is opened. If one photon is emitted by a radioactive source in the respective direction, it can deposit its energy in one of those materials. A defined fraction of this deposited energy will be emitted again and possibly seen by the detector setup. In Table 1.1 the energies of the emitted radiation (Firestone et al., 1999) for the radioactive sources as well as the fluorescence lines are listed. The materials have been chosen such that the energy lines are spread over a large area of the sensitive energy range of the detector setup to allow for a good energy calibration.

The setup contains a piston pump and a turbomolecular pump to reach a vacuum with a remaining pressure of $P \approx 10^{-7}\,\mathrm{mbar}$. As soon as the pressure falls below $P \approx 10^{-2}\,\mathrm{mbar}$ the cooling system can be started without any condensation effects. To reduce the noise of both detectors the temperature should be below $T \approx -40\,^{\circ}\mathrm{C}$. The cooling system is a heat exchanger which can reach a minimal temperature of $T \approx -80\,^{\circ}\mathrm{C}$. The data of both detectors are transmitted via SpaceWire to a computer station. With a software called “Idef-X”, commands can be sent from the computer station to the detectors and the incoming data can be stored.

Table 1.1: The photon energies emitted by the radioactive sources of the CANDELA setup are shown in this table as well as the fluorescence lines according to Firestone et al. (1999). Note that in the column "source" the initial elements are listed. For the radioactive sources, some energies are emitted from other elements after the decay. The elements marked with † are the materials emitting fluorescence lines.

Source	Energy [keV]	Source	Energy [keV]	Source	Energy [keV]
Al†	1.49	Am	13.95	Am	21.10
Ti†	4.51		15.86		21.34
	4.93		16.11		21.49
Fe	5.90		16.82		26.35
	6.49		17.06		33.20
Cu†	8.04		17.51		43.42
	8.91		17.75		59.54
Am	11.87		17.99		
	13.76		20.78		

1.2.1 The Low Energy Detector (LED)

The LED is a DEPFET[1] detector made of silicon and has an energy resolution of $\Delta E = 168\,\text{eV}$ FWHM at 6 keV. The quantum efficiency of a silicon detector is roughly given in the energy range between 0.1 keV and 15 keV[2] and thereby only a small fraction of photons in the hard X-ray range which is located at energies above the upper limit of 15 keV will be detected. The LED is positioned 10 mm in front of the HED and has a distance to the radiation sources of $\Delta z = 230\,\text{mm}$. The LED is logically subdivided into a matrix of 64×64 pixels where each pixel has a size of $500\,\mu\text{m} \times 500\,\mu\text{m}$ (see Figure 1.2). The readout of the pixels is realized by a CAMEX chip[3] after a defined frame time. All pixels are read out individually in one cycle in which the collected charges in the semiconductor are transformed into electrical signals. This readout procedure takes a total time of $T_{\text{frame}} \approx 2.4\,\text{ms}$ which is considered the time resolution in full frame operation mode.

The setup is able to perform a real-time data preprocessing which means

[1] A DEPFET (depleted p-channel field-effect transistor) is an electrical semiconductor device which can be used to detect photons and charged particles.

[2] The limits of this range can not be given exactly because the quantum efficiency increases or decreases in a certain region around those values. Additionally, those limits are depending on the thickness of the silicon detector.

[3] See Herrmann et al. (2008) for further information of CAMEX readout chips.

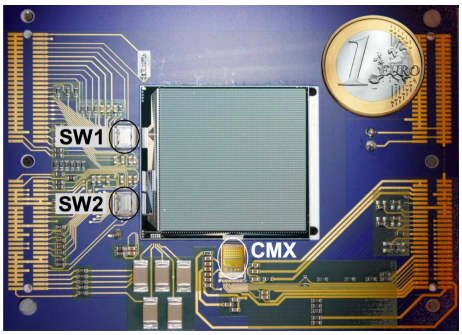

(a) A view of the LED and the readout electronics with a 1 Euro coin for scale.

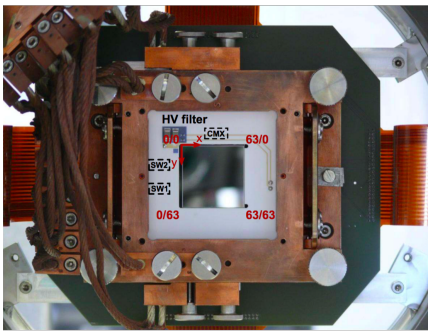

(b) A view of the illuminated side of the LED. In red you see the coordinate system of the pixel matrix.

Figure 1.2: The low energy detector of the CANDELA setup. Images: Maier (2015)

that not all recorded data will be sent to the computer. This is necessary to minimize the amount of data which has to be transmitted to make sure that no information is lost because the pipeline is overloaded. There are several criteria a data set (all information coming from one pixel) has to fulfill before it is signed as a legal event. Only legal events will be transmitted and saved.

- **Energy range:** The value of the measured pulse height amplitude (PHA) in a given pixel has to be above a defined threshold to exclude events caused by noise. But this threshold should not be set too high, otherwise the spectrum will have a reduced flux and a cutoff at low energies. One photon can split its initial energy between up to four pixels. To register all pixels of such split events even with a low PHA in a neighbour pixel, there is an additional threshold for the neighbour pixels of valid events. A third PHA value defines the upper end of the energy range to prevent MIPs[4] from being marked as legal events.

- **Pattern recognition:** A split event is legal if its initial photon deposits energy in up to three adjacent pixels depending on the impact position of the photon. There is a pattern recognition which looks for illegal split events with more than three adjacent pixels or an invalid geometry (for example three pixels in a row). This analysis

[4]MIPs (Minimum Ionizing Particles) are secondary particles coming from the interaction between cosmic rays and either the atmosphere of the Earth, the detector or the satellite. Those particles lose just a small fraction of their energy by interacting with the detector but still enough to leave signals in all pixels crossing their way.

also prevents MIPs from being transmitted if they leave their energy distributed over several pixels in their trace through the detector. But in some cases illegal events can not be identified, for example if there are two low energetic photons in the same or in adjacent pixels. In this case the total energy of both events is assigned to only one photon (pile up).

- **Bad pixels:** Some pixels are defect and have constantly very high (hot pixels) or very low (cold pixels) count rates. To find such pixels, a measurement without any sources can be done. In this case each pixel should have in average the same count rates caused by background. After such a measurement, hot and cold pixels can be marked in a bad map and they will no longer transmit any data.

For the remaining events there are corrections to do before the data will be sent to the computer. An **offset correction** is a pixel individual value subtracted from the measured PHA. Those values are stored in the offset map and can be transmitted from the computer to the detector setup. After this, a **Common-mode correction** can be done. This is necessary because there are variations of the supply voltages of the CAMEX chip for the pixel rows which results in a common offset of each pixel in the respective row. The common-mode can be set to the median of its pixel row. This value is subtracted from each pixel of the corresponding row. After this correction, the pixels without events will have a PHA distribution around the value zero.

Each transmitted legal event will have 8 bytes of information: time, PHA, pixels and several flags. See Table 1.2 for the detailed data composition. There is also a primary byte which signalizes a scientific data transfer (0x35). After the 8 bytes there is also one more marker to note the end of a correct data package (0x100) or the end of an incorrect data package (0x101).

During the analysis, the binary data has to be translated from the data structure according to Table 1.2 into a fits file[5]. After this, the legal split events have to be identified and recombined into a single event. An energy calibration can be done by using the energies listed in Table 1.1 to transform the PHA into real energies.

[5]A fits (flexible image transport system) file is commonly used in astronomy to handle scientific data. Each file contains columns sorted by the type of the respective information. With e.g. the data handling software "fitsview" it is possible to visualize one or more of those columns in plots.

Table 1.2: Structure of the transmitted LED data packages. The scientific data of the LED has a defined structure for the time, PHA, pixels and several flags. In this table the amount of bits assigned to the different kinds of information are shown.

Information	Time [s]	Time [10^{-7} s]	PHA [ADU]
Bits	8	24	14
Information	Pixel x	Pixel y	Flag
Bits	6	6	6

1.2.2 The High Energy Detector (HED)

The HED is a Schottky device[6] consisting of a thin platinum plate, a cadmium telluride (CdTe) semiconductor and aluminium contacts of the pixels (see Figure 1.3). The CdTe detector has an energy resolution of $\Delta E = 1050\,\text{eV}$ FWHM at 60 keV. The quantum efficiency of the HED increases at about 2 keV and decreases again at approximately 100 keV and is thereby a good addition to the LED which is sensitive up to 15 keV. There are 8×8 pixels with a size of $1\,\text{mm} \times 1\,\text{mm}$ per pixel.

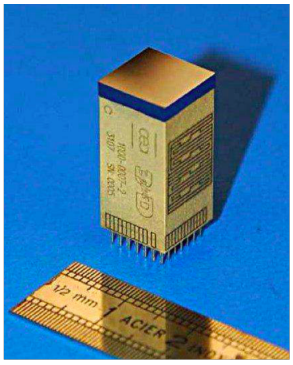

(a) The HED in comparison with a length scale. Image: Meuris et al. (2009)

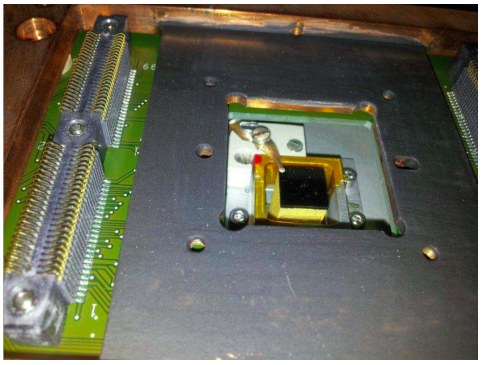

(b) The HED installed at its position 10 mm behind the LED which is not installed in this picture. Image: Maier (2015)

Figure 1.3: The high energy detector of the CANDELA setup.

The readout procedure of the HED is completely different compared to the LED. Each pixel of the HED can trigger a readout when its signal

[6] A Schottky diode has a junction of a semiconductor and a metal. This causes a lower forward voltage drop compared to usual semiconductor diodes.

exceeds a defined threshold. Signals triggered by noise can be suppressed with a continuous discharge of each pixel. This also results in an event signal without any offset in the PHA. The measured time resolution of the HED events of $\sim 70\,\mu s$ is small compared to the time resolution of the LED events which is given by the frame time $T_{\text{frame}} \approx 2.4\,\text{ms}$. 16 pixels are combined in one ASIC (Application Specific Integrated Circuit), which means that there are four ASICs for all 64 pixels. There is a total amount of 49 input and output ports for the voltage supplies, parameters (for example the energy threshold) and the signal output.

There is the same scientific information for the HED transmitted as for the LED: x and y position, the PHA and the event time. But the structure of a data package is not the same because of the different read out procedure. The data package consists of two parts: a header with basic information e.g. the type of data or the respective time and a second part from the ASICs with specific information on the pixel events. At the beginning of a data package there is a byte assigned with 0xFE and one more byte to identify a scientific data package with 0xF5. At the end of the data package there is an extra byte which signalizes the end of the package with a value different from 0x00. See Table 1.3 for details of the transmitted data structure.

Table 1.3: The scientific data of the HED transmitted to the computer station have a defined structure for the frame, time, PHA and ASIC information. In this table you see the amount of bits assigned to the different kinds of information. Note that not the entire data package is listed here. The table is limited to the relevant data used for the event analysis.

Information	Frame	Time [s]	Time [10^{-8} s]
Bits	8	5	27
Information	PHA [ADU]	ASIC number	Channel number
Bits	16	4	4

It is possible to translate the ASIC and channel number into the x and y position of the pixel. The ASIC number labels the event to come from one of the 16 pixels of the respective ASIC. With the four bits of the channel number the exact pixel of the event can be determined. The energy calibration of the HED is performed similar to the LED by using the energies listed in Table 1.1.

1.2.3 The stacked system of the LED and HED

The stacked system of the LED and HED can be studied to enable new applications of the combined setup. To make a spatial analysis of the events in the LED and HED, a global coordinate system (GCS) should be defined. As shown in Figure 1.4 the GCS was chosen to have its origin in the center of the LED with two axes parallel to those of the LED. The third axis is orthogonal to those and points in the direction of the HED to realize a right-handed coordinate system.

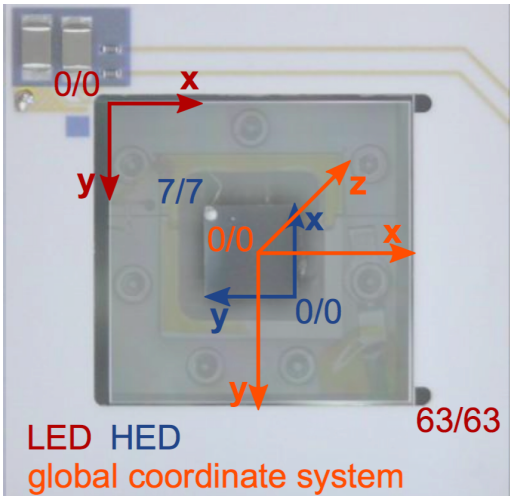

Figure 1.4: Coordinate systems of the LED, HED and the global system. The global coordinate system (GCS) has its origin in the center of the LED (shown in orange). The x and y axes are chosen parallel to those of the LED. To obtain a right-handed system the additional z axis needs to point in the direction of the HED. Image: Maier (2015)

It can be expected that the detectors will have influences on each other when they are used in the stacked operation. For example, there are heating effects which result in a higher noise compared to a single run of one detector. Another point are spectral changes in both detectors because of effects like fluorescence lines or the spectral cutoff in the HED at low energies because of the overlapping quantum efficiencysensitivity of the detectors.

But there are not only adverse features. For example, fluorescence lines or scattered events can be used to synchronize the time information of both detector systems. One energetic photon may leave its energy in the HED and a fluorescence photon will be emitted. If this photon will be detected in the LED this event can be reconstructed. Since the distance between the LED and HED is only 10 mm, the time difference between the interactions in the LED and HED is negligible small compared to the time

accuracy of the detectors which enables a precise time synchronization. Additionally, the detector system has a very high quantum efficiency (close to 100 %) between 0.1 keV and 100 keV which is a larger range compared to *XMM-Newton* or *Chandra* (Zombeck, 2007) combined with a great energy resolution of 168 eV FWHM at 6 keV and 1050 eV FWHM at 60 keV. Furthermore, the idea of stacked detectors also opens new possibilities for future X-ray instruments as the setup is able to record Compton scattering events which will be shown and analyzed in Chapter 3.

Chapter 2

CASIMEO - an NRTA software

The CASIMEO (**C**ANDELA **a**nalysis **s**oftware **im**aging **e**vents **o**nline) software is a Python script[1] implemented to realize a near real-time analysis (NRTA) software which can analyse and display the scientific data transmitted to the computer while one or both detectors are still in an operation mode. The data are saved by the "Idef-X" software in .tm files with a size of 2 Mbyte each. As soon as one file has reached this size, a new file will be created and the CASIMEO software starts to analyse the completed file. The software is able to show up to four plots for each detector.

- **Hitmap:** The hitmap shows the pixel matrix (64×64 pixels for the LED or 8×8 pixels for the HED) with the number of detected events in each pixel. This number is illustrated by different colors in a logarithmic scale.

- **Hitrate (frames):** The entire amount of events summarized over all pixels per frame can be plotted. For the LED, one frame is associated with the time information of an event manually by the frame time $T_{\text{frame}} \approx 2.4\,\text{ms}$ while the data for the HED already contains the frame information (see Table 1.2 and Table 1.3).

- **Hitrate (time):** In addition to the hitrate in units per frame, a hitrate in units per time was implemented which shows the amount of events collected in one second.

- **PHA spectrum:** The PHA spectrum is a histogram with 1000 bins. The data from the LED have 14 bits while the data from the HED

[1] The Python script was written for Python 2.7 and a Linux operating system but in principle it can be adapted for other operating systems as well.

have 16 bits available for the PHA information. This results in a PHA range for the LED between 0 and $\sim$ 16000 and for the HED between 0 and $\sim$ 65000.

Note that split events are not analysed in the plots shown by default which means that one photon can cause events in up to four pixels which appears in higher values in the hitmap as well as in the hitrates. Such an unidentified split event also modifies the PHA spectrum by splitting the PHA value caused by the initial photon in up to four PHA values.

CASIMEO can be run in a single mode for the LED or the HED as well as in a common mode for both detectors. The software can be started with a terminal calling the Python script and optionally six or eleven parameters for the single or common operation mode. For the single operation mode there are one parameter for the operation mode, four parameters for the shown plots and one parameter for the path of the LED or the HED files (see Table 2.1). The operation mode parameter can be set to the values LED or HED which implies five more parameters to follow. The next four values activate (1) or deactivate (0) the corresponding plots with the default value of 1. The last parameter has to be set to the path of the LED or HED files starting from the placement of the Python script. For example, a single operation mode of the CASIMEO software could be started with

```
python CASIMEO.py LED 1 0 1 1 Data_LED/          (2.1)
```

to analyse the LED data stored in the assigned folder.

Table 2.1: The six parameters of the CASIMEO single operation mode are shown in this table. The parameter 1 declares the operation mode, the parameters 2 to 5 show or hide the respective plot and the parameter 6 is the path of the LED or HED files. There is no default value for the parameter 1 because the common operation mode (see Table 2.2) would be chosen in default.

Parameter	Function	Values	Default value
1	Operation mode	LED or HED	–
2	Hitmap	0 or 1	1
3	Hitrate (frames)	0 or 1	1
4	Hitrate (time)	0 or 1	1
5	PHA spectrum	0 or 1	1
6	Path of files	pathoffiles/	./

Similar to the single operation mode, the common operation mode can be called. Therefore, the operation mode parameter has to be set to LED-HED. In this mode, the next eight parameters can be chosen to show or hide the respective plots and the last two parameters assign the paths of the LED and the HED files (see Table 2.2). To start a common operation mode the Python script could be called with

```
python CASIMEO.py LEDHED 1 0 1 1 1 0 1 1 LED/ HED/   .    (2.2)
```

Table 2.2: The eleven parameters of the CASIMEO common operation mode are shown in this table. The parameter 1 declares the operation mode, the parameters 2 to 9 show or hide the respective plots and the parameters 10 and 11 are the paths of the LED and the HED files.

Parameter	Function	Values	Default value
1	Operation mode	LEDHED	LEDHED
2	LED Hitmap	0 or 1	1
3	LED Hitrate (frames)	0 or 1	1
4	LED Hitrate (time)	0 or 1	1
5	LED PHA spectrum	0 or 1	1
6	HED Hitmap	0 or 1	1
7	HED Hitrate (frames)	0 or 1	1
8	HED Hitrate (time)	0 or 1	1
9	HED PHA spectrum	0 or 1	1
10	LED path of files	pathofLEDfiles/	./
11	HED path of files	pathofHEDfiles/	./

In the common operation mode CASIMEO starts with the analysis of the LED data. As soon as the analysis of one file is done, the chosen plots will be updated. If there is already a new file with LED data, the software will continue automatically with the analysis. Otherwise, the script would continue with the analysis of the HED files. If there are no more files to analyse, the software will wait for 5 seconds before it checks the respective folders again. For the single operation mode, there is the same progression for one of the detectors. “Ctrl + c” can be pressed to stop the analysis of further data but allows still to study the shown plots. To end the software and close all plots at once, the “return” key can be pressed.

2.1 LED data analysis

The CASIMEO software was tested by taking a measurement with an IAAT logo mask between the sources and the detectors. Figure 2.1 shows the LED hitmaps after each analysed file. The default color was chosen to be black

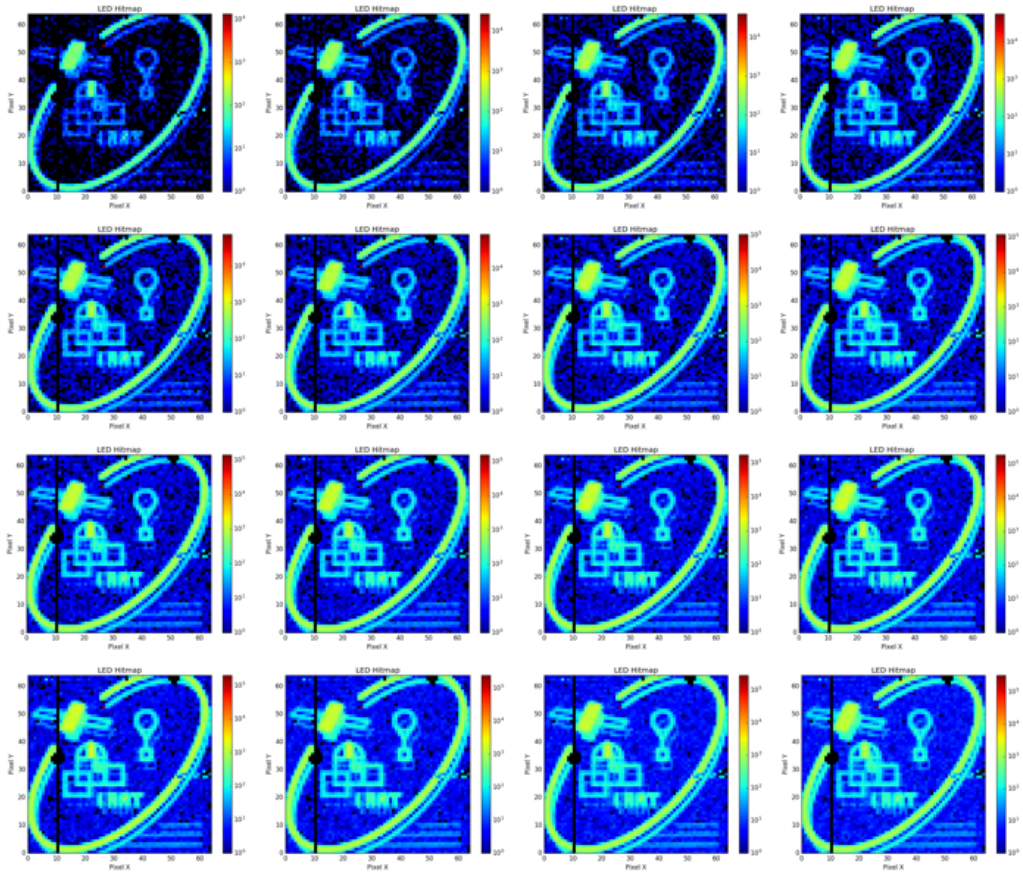

Figure 2.1: The LED hitmap is shown for a data set of 16 files. There was a mask with the IAAT Logo between the sources and the detectors, which can be seen in the plots very well. In the last plot, there are still pixels without any events that are colored in black. Most of them were marked as hot or cold pixels in the bad map, for example the entire pixel column 11. The pixel $(27, 53)$ with a value of about two orders of magnitudes higher compared to the others causes a shift to lower colors. This pixel will be added to the bad map in further measurements.

for the pixels with zero events in the logarithmic scale. In the last hitmap, there are still some black coded pixels, for example the entire pixel column 11. Those pixels were marked as hot or cold pixels in the bad map and

therefore no data were transmitted from the setup for those pixels. In the last shown hitmap of Figure 2.1 the range of the detected photons is located between 0 and 3×10^5. There was a total amount of 8×10^5 events detected in all pixels. In the IAAT logo of the used mask, there is actually only one ring to illustrate the satellite orbit instead of the two rings that can be seen in Figure 2.1. The second ring is the result of the different positions of the X-ray sources in the CANDELA setup. Shortly after the beginning of the measurement, the sources were swapped by the mechanical shutter to release all energies listed in Table 1.1 to enable a better energy calibration.

Figure 2.2 to Figure 2.5 show the results of a measurement which was used for the analysis of identified Compton events presented in Chapter 3. The LED was operated with eight pixel rows only to reduce the required time of the readout procedure by a factor of 1/8 which results in a better time resolution of the detected LED events of $\sim 0.3\,\mathrm{ms}$ which is important for an analysis of Compton events. The 64×8 pixels detected between 492 and 7651 events each and a total number of 1.8×10^6 events. The column 11 and pixel $(64, 3)$ had been marked in the bad map.

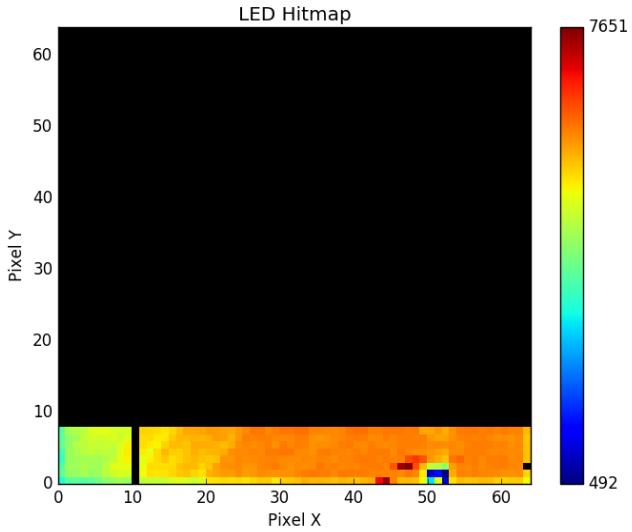

Figure 2.2: The hitmap of the LED is shown in this figure. Each pixel of the 64×64 pixel matrix has a color coded value in a logarithmic scale. The LED was operated with eight pixel rows only to increase the time resolution of the detected events.

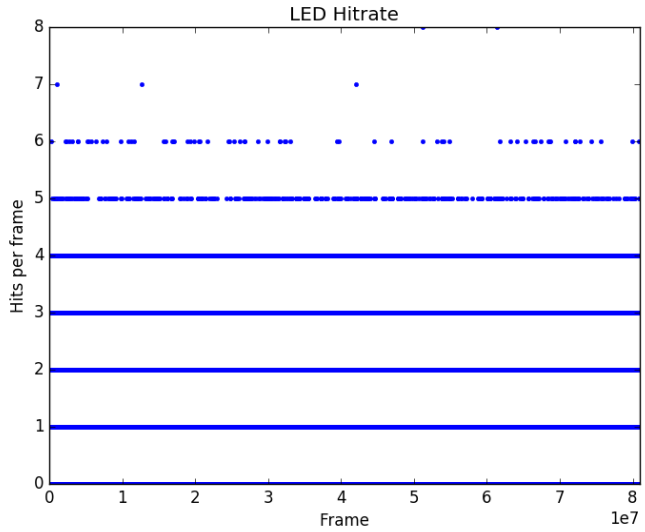

Figure 2.3: The hitrate of the LED in units per frame is shown in this figure. There is a total number of about 8×10^7 frames with a maximum of 8 events per frame.

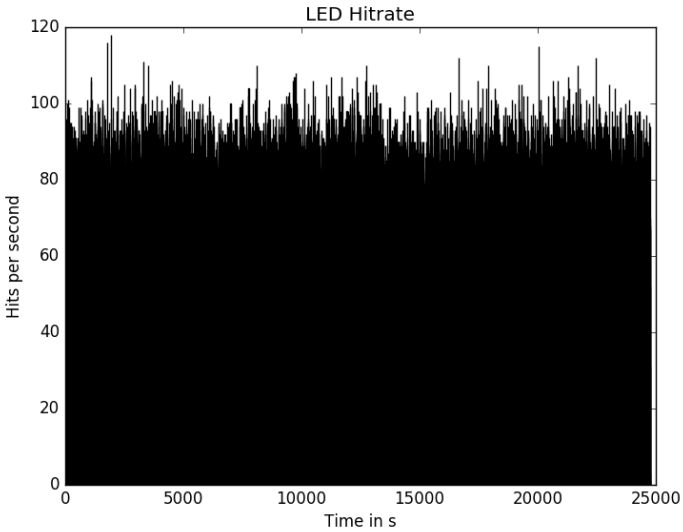

Figure 2.4: The hitrate of the LED in units per time is shown in this figure. The values are presented in a histogram with a binsize of one second each. During the measurement of about 25 ks, there was an average count rate of 73 hits per second.

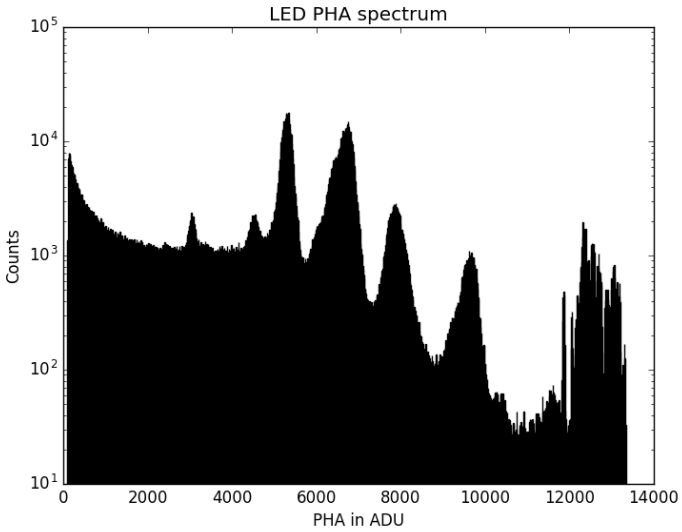

Figure 2.5: The PHA spectrum of the LED is shown in this figure as a histogram with 1000 bins. There are six peaks in the range from 3000 ADU to 10 000 ADU which can be used for an energy calibration.

The hitrate of the LED in units per frame is shown in Figure 2.3 with an average of 0.02 events per frame and a highest value of 8 events per frame. Note that one photon can cause a signal in up to four pixels what possibly had shifted the hitrate to higher values. The hitrate in units per second is shown in Figure 2.4. The measurement over a time of $t \approx 25\,\mathrm{ks}$ had an average hitrate of $\lambda = 73$ hits per second. The variations of the hitrate can be explained by the statistical behaviour of the radioactive sources which produce photons at a rate following a Poisson distribution[2]. The standard deviation σ of a Poisson distribution is given by

$$\sigma = \sqrt{\lambda} = 8.5 \quad . \tag{2.3}$$

For a confidence interval of 3σ, about 99.7 % of the values should be placed within this interval which is in a good agreement compared to the values shown in Figure 2.4. Note that the histogram seems to show a higher hitrate which is a result of the high amount of 25 000 bins.

The PHA spectrum of the LED is shown in Figure 2.5. There are at least six peaks which can be used for an energy calibration. With the method described in Subsection 3.2.2, the energy calibration can be done with even more reference points than expected according to Figure 2.5.

[2]See Fornasini (2008) for an introduction to statistics occurring in physical measurements.

2.2 HED data analysis

The measurement of the presented results of the LED (Figure 2.2 to Figure 2.5) was done with both detectors operating at once. Figure 2.6 to Figure 2.9 show the results of this measurement for the HED. The hitmap with the 8×8 pixel matrix is shown in Figure 2.6. After the measurement, the HED pixels had registered in average 49 600 events and a total amount of 3.2×10^6 events. Since the pixel $(4, 5)$[3] had a significant higher value compared to the other 63 pixels, this pixel was excluded for the calculation of the average amount of events.

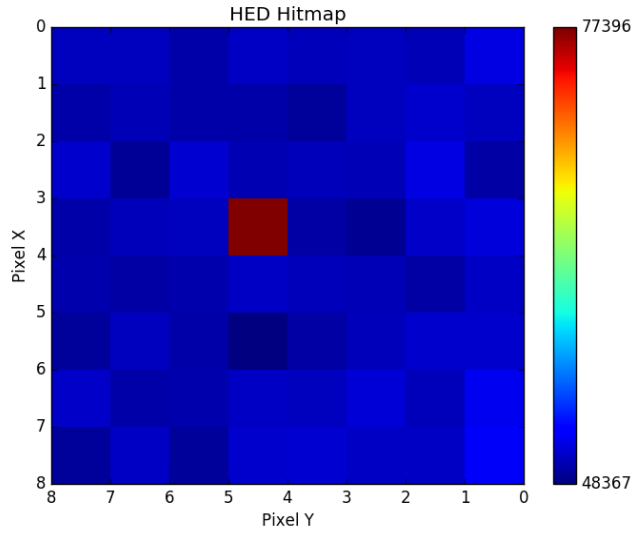

Figure 2.6: The hitmap of the HED is shown in this figure. Each pixel of the 8×8 pixel matrix has a color coded value in a logarithmic scale. Note the selection of the axes which were chosen to have the same orientation as the LED coordinate system.

Figure 2.3 shows the hitrate in units per frame with a total amount of 2.9×10^6 frames. There are frames with outstanding values of 20, 15 or 14 hits per frame what is unexpected for the HED because of its readout procedure which was explained in Subsection 1.2.2.

The hitrate in units per time is shown in Figure 2.8 with a total observation time of $t \approx 25\,\text{ks}$. The polarization effect of the CdTe detector, which was discussed for example by Nadege et al. (2010), could be reduced

[3]Note that the x-pixels are plotted at the y axis and the y-pixels are plotted at the x axis in an inverse way. This was done to make the axes of the HED coordinate system parallel to the axes of the LED coordinate system.

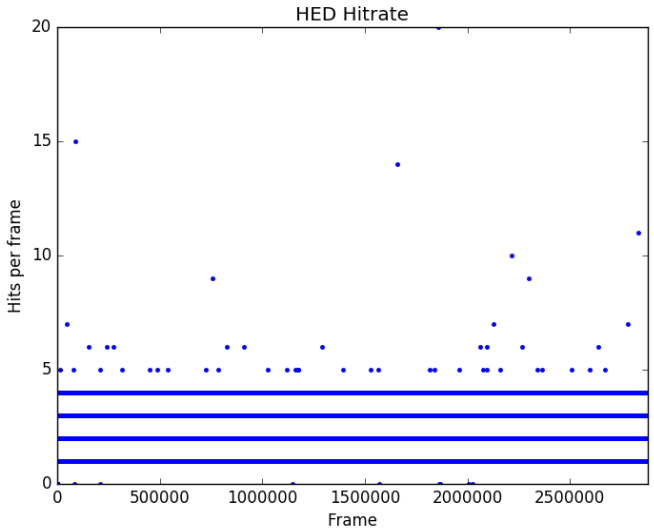

Figure 2.7: The hitrate of the HED in units per frame is shown in this figure. There is a total amount of 2.9×10^6 frames and the highest value had one frame 20 hits.

by turning off the supply voltage of the HED for two time intervals. This results in the two drops in the hitrate between 9030 s and 9170 s and the second one between 15 900 s and 16 220 s. The increase of the hitrate at the end of the measurement above 23 200 s can not be attributed to changes in the operation sequence and is as of yet unexplained.

Figure 2.9 shows the PHA spectrum of the HED. The majority of the detected events is located at PHA values between 200 ADU and 1450 ADU and in this range it is possible to perform an energy calibration with the present peaks. For PHA values above 1450 ADU, there are just a few counts without any significant peaks. According to Table 1.2 and Table 1.3, the available amount of bits for the transmission of the PHA data are 14 bits for the LED and 16 bits for the HED. Comparing the PHA ranges of the LED and the HED shown in Figure 2.5 and Figure 2.9, it can be seen that the used PHA range of the HED is about 8000 ADU smaller than the PHA range of the LED. Therefore, the gain of the HED could be increased for further measurements to increase the PHA sensitivity of the HED.

Since a measurement is done, the near real-time data analysis realized by CASIMEO can be continued by an offline data analysis. As already presented in Section 1.2, a pattern recognition can look for split events and combine them to one event. Additionally, the .tm files can be converted

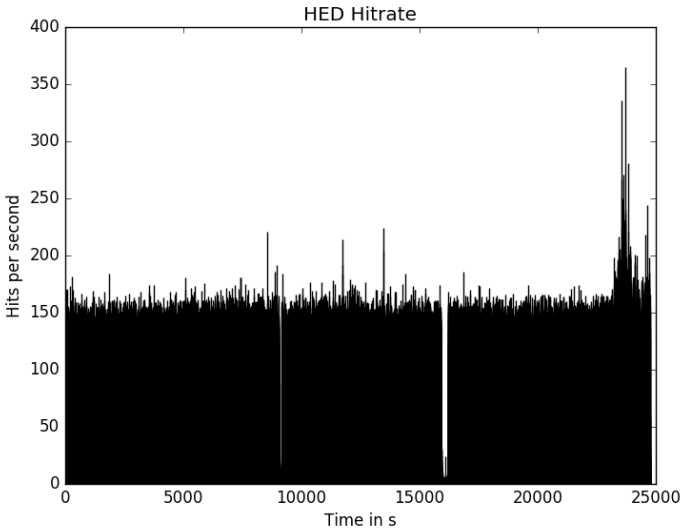

Figure 2.8: The hitrate of the HED in units per time is shown in this figure. The values are presented in a histogram with a binsize of one second each. During the measurement of about 25 ks, there was an average count rate of 132 hits per second.

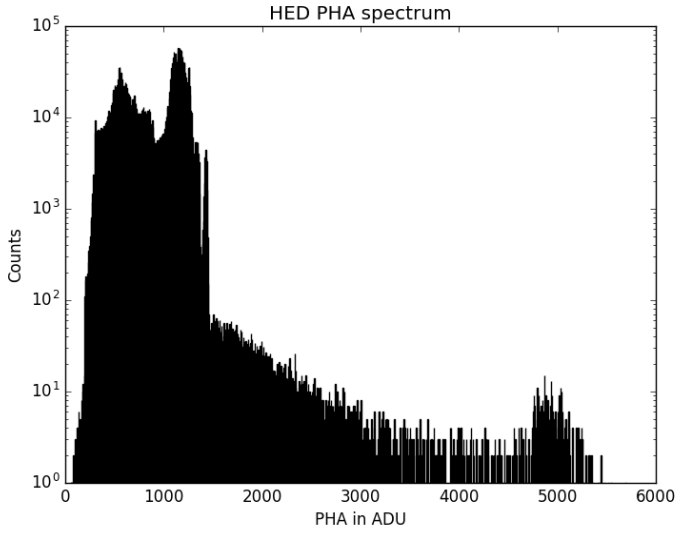

Figure 2.9: The PHA spectrum of the HED is shown in this figure as a histogram with 1000 bins. There are many events at the left-hand side of the histogram, but the amount of detected events decreases rapidly for higher PHA values which can be explained by the decreasing quantum efficiency of the HED. The events on the right-hand side could be caused by pile up events or statistical fluctuations.

to one fits file for the LED and one for the HED events. Furthermore, an energy calibration for both PHA spectra can be executed, which is explained in Subsection 3.2.2. For the CANDELA setup, this offline analysis was implemented by Maier (2015). On the basis of this offline analysis, a software was implemented to analyse Compton scattering events which is presented in the following Chapter 3.

Chapter 3

Application as a Compton camera

Compton scattering is an interaction between a photon and a quasi free electron. For this interaction, an expression for the scattering angle between the photon and the electron Θ should be found. Assuming that the electron is in a rest frame, the energy transfer from the photon to the electron can be described according to Longair (2012) with

$$\lambda' - \lambda = \frac{h}{m_\mathrm{e} c} \left(1 - \cos\Theta\right) \quad , \tag{3.1}$$

where λ is the wavelength of the photon before the scattering process, λ' is the wavelength of the photon after the scattering process, h is the Planck constant, m_e is the mass of the electron and c is the speed of light. Using the relation of the wavelength to the photon energy

$$E = h\nu = h\frac{c}{\lambda} \tag{3.2}$$

$$\lambda = \frac{hc}{E} \quad , \tag{3.3}$$

where E is the energy of the unscattered photon, equation (3.1) can be written as

$$hc\left(\frac{1}{E'} - \frac{1}{E}\right) = \frac{h}{m_\mathrm{e} c} \left(1 - \cos\Theta\right) \tag{3.4}$$

$$\frac{1}{E'} - \frac{1}{E} = \frac{1}{m_\mathrm{e} c^2} \left(1 - \cos\Theta\right) \tag{3.5}$$

$$\cos\Theta = m_\mathrm{e} c^2 \left(\frac{1}{E} - \frac{1}{E'}\right) + 1 \quad , \tag{3.6}$$

where E' is the energy of the scattered photon. Since a stacked detector system is able to determine the energies E and E' (see Section 3.1), the

scattering angle Θ can be calculated. This angle Θ defines a cone with a circle as base where the origin of the photon can be located on its surface. For an ensemble of photons emitted from the same source, all of those circles overlap in one point which is equal to the position of this source. For a Compton camera, this overlap only occurs for the correct distance from the LED to the source plane. For smaller distances, this position would be outside of each ellipse[1] and for larger distances it would be inside the ellipses and thus a correct reconstruction of the position of the source would not be achievable. That is why a possible application of a Compton camera could be to compute the position of a nearby point-like, isotropically emitting X-ray or gamma source in three dimensions.

The idea of using Compton scattering events for astronomical observations has already been realized several times. The imaging Compton telescope[2] (COMPTEL) on board of the *Compton Gamma-Ray Observatory* (GRO) for example used Compton events in the energy range between 1 MeV and 30 MeV to perform an all sky survey at MeV energies (Schoenfelder et al., 1993). Another example was the Japanese satellite *HITOMI* (previous called *ASTRO-H*) which had a Compton telescope made of silicon and cadmium telluride on board (Ichinohe et al., 2016) and thereby used the same detector materials as the CANDELA setup. Unfortunately, the *HITOMI* satellite had only a few weeks lifetime after its launch in 2016.

3.1 Compton scattering in the CANDELA setup

A Compton scattering event in the CANDELA setup can be detected if a photon is scattered in the LED and the scattered photon is absorbed completely in the HED[3] as shown in Figure 3.1. In this case, the initial energy of the photon can be determined. According to equation (3.6), the scattering angle Θ can be calculated if the energies E and E' are known. For the CANDELA setup, those energies are given by

$$E = E_{\mathrm{LED}} + E_{\mathrm{HED}} \qquad \text{and} \qquad E' = E_{\mathrm{HED}} \quad . \tag{3.7}$$

[1] For finite distances between the detector and the source plane, the circles project ellipses onto the source plane.

[2] The difference between a Compton camera and a Compton telescope is the distance of the observed source. While Compton cameras have a look at nearby sources, a Compton telescope observes objects in an "infinite" distance.

[3] In principle, it is also possible for photons to get Compton scattered in the HED and to be absorbed in the LED. But according to Maier (2015), the geometrical and material properties of the CANDELA setup are not suitable for such Compton back scattering events.

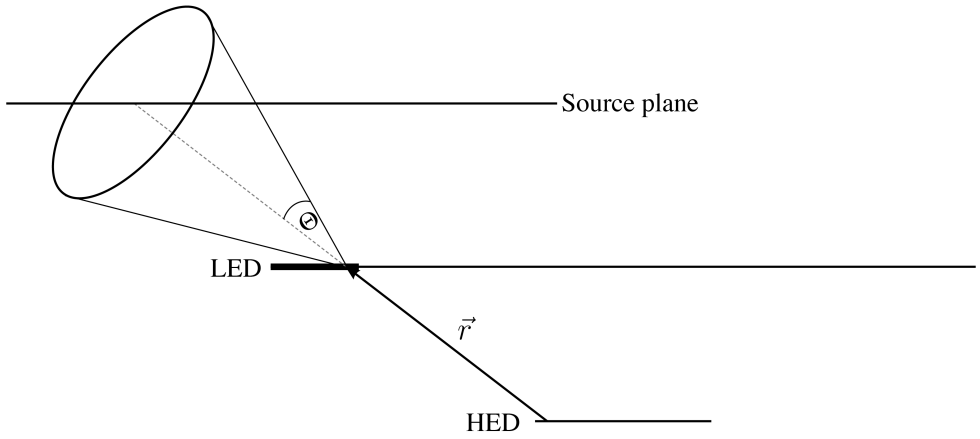

Figure 3.1: The Compton scattering geometry of the CANDELA setup. A photon coming from the source plane can be Compton scattered in one of the 8 operating pixel rows of the LED with the angle Θ and be absorbed in the HED. The origin of the photon can be reconstructed with a circle by projecting the circle on the source plane. The resulting ellipse at the intersection with the source plane are the possible origins of the photon. The direction vector $\vec{r}$ is the line between the interaction points in the LED and HED and defines the middle of the circle. Note that the distances between the detectors and the source plane are not scaled correctly for illustration reasons.

The calculated scattering angle

$$\Theta = \arccos\left(m_{\mathrm{e}}c^2\left(\frac{1}{E_{\mathrm{LED}}+E_{\mathrm{HED}}}-\frac{1}{E_{\mathrm{HED}}}\right)+1\right) \tag{3.8}$$

is also the aperture angle of the cone shown in Figure 3.1. The direction vector $\vec{r}$ is the line between the interaction points in the LED and HED and defines the middle of the circle.

For the CANDELA setup, an analysis of Compton events was implemented to trace back the initial photons to the source they came from. Before this analysis can be done, the data of the Compton events have to be preprocessed which will be explained in Section 3.2. The Compton analysis itself will be presented in Section 3.3 followed by the results of a measurement in Section 3.4.

3.2 Data preprocessing

As a first step, the coordinates of the LED and HED events have to be transformed to the GCS (Subsection 3.2.1), the energies of both detector events have to be calibrated (Subsection 3.2.2) and the time of the LED and HED has to be synchronized (Subsection 3.2.3).

3.2.1 Coordinate transformation

For describing the Compton scattered photons, a global coordinate system (GCS) was defined. To transform the coordinates of the LED and HED to the GCS, the pixel information has to be converted into a consistent length. Since the origin of the GCS was chosen to be in the center of the LED and the axes were defined to be parallel compared to the axes of the LED, the coordinates can be transformed into a length scale in mm with

$$x_{\mathrm{LED}} = (x_{\mathrm{LED}}^{\mathrm{pix}} - 31.5) \cdot 0.5\,\mathrm{mm} \quad , \tag{3.9}$$

$$y_{\mathrm{LED}} = (y_{\mathrm{LED}}^{\mathrm{pix}} - 31.5) \cdot 0.5\,\mathrm{mm} \quad , \tag{3.10}$$

for the size of one LED pixel of $0.5\,\mathrm{mm} \times 0.5\,\mathrm{mm}$. $(x_{\mathrm{LED}}^{\mathrm{pix}}, y_{\mathrm{LED}}^{\mathrm{pix}}, z_{\mathrm{LED}}^{\mathrm{pix}})$ are the pixel values of the events and $(x_{\mathrm{LED}}, y_{\mathrm{LED}}, z_{\mathrm{LED}})$ are the corresponding coordinates in the GCS. The transformation was chosen in a way that the position in the GCS is located in the middle of the respective pixel. With a number of 64×64 pixels the center of the LED is positioned at $(32, 32)$. To calculate the position in the middle of each pixel, the value 0.5 has to be subtracted from both coordinates which results in the presented offset of $(-31.5, -31.5)$. The third component is $z_{\mathrm{LED}} = z_{\mathrm{LED}}^{\mathrm{pix}} = 0$ for all LED events.

The transformation of the HED pixels into the GCS is similar to the transformation of the LED coordinates. With 8×8 pixels and a size of $1\,\mathrm{mm} \times 1\,\mathrm{mm}$ per pixel, the transformation can be done with

$$x'_{\mathrm{HED}} = (3.5 - y_{\mathrm{HED}}^{\mathrm{pix}}) \cdot 1\,\mathrm{mm} \quad , \tag{3.11}$$

$$y'_{\mathrm{HED}} = (3.5 - x_{\mathrm{HED}}^{\mathrm{pix}}) \cdot 1\,\mathrm{mm} \quad . \tag{3.12}$$

Note that according to Figure 1.4, the x-axis of the HED is parallel to the y-axis of the GCS and the y-axis of the HED is parallel to the x-axis of the GCS. Since the center of the HED is shifted with respect to the origin of the GCS by $(-1.42\,\mathrm{mm}, -0.01\,\mathrm{mm})$ as calculated by Maier (2015), the coordinates of the HED have to be corrected with

$$x''_{\mathrm{HED}} = x'_{\mathrm{HED}} - 1.42\,\mathrm{mm} \quad , \tag{3.13}$$

$$y''_{\mathrm{HED}} = y'_{\mathrm{HED}} - 0.01\,\mathrm{mm} \quad . \tag{3.14}$$

Maier (2015) also measured that the HED is misaligned by an angle of $\alpha = 0.74\,^\circ$. With the rotation matrix in two dimensions

$$R_2(\varphi) = \begin{pmatrix} \cos\varphi & -\sin\varphi \\ \sin\varphi & \cos\varphi \end{pmatrix} \tag{3.15}$$

this misalignment can be corrected with the rotation of the coordinates by an angle of $-\alpha$

$$\begin{pmatrix} x_{\mathrm{HED}} \\ y_{\mathrm{HED}} \end{pmatrix} = \begin{pmatrix} \cos\alpha & \sin\alpha \\ -\sin\alpha & \cos\alpha \end{pmatrix} \cdot \begin{pmatrix} x''_{\mathrm{HED}} \\ y''_{\mathrm{HED}} \end{pmatrix} \quad . \tag{3.16}$$

The third component of the HED events is given by the distance between the LED and HED of $z_{\mathrm{HED}} = 10\,\mathrm{mm}$.

3.2.2 Energy calibration

The energies of the LED and the HED events have to be calibrated to enable the calculation of the Compton scattering angle (see Equation (3.8)). Therefore, the energy lines of the CANDELA sources of Table 1.1 can be used. For the energy calibration, the implemented software of Maier (2015) was used.

This software locates the expected peaks and writes the corresponding PHA values into an extra file for each pixel. Since not all of the energy peaks are really prominent, a rough energy calibration can be done for the most dominant peaks first. Then, the less dominant peaks can be searched at the expected energies and a more precise energy calibration can be performed. After the expected peaks are found pixel individually, the PHA values can be associated with the energy values which is done with a cubic spline interpolation[4]. For the HED, a spline interpolation can not be done because there are not enough calibration peaks in the energy range of the HED. Instead of a spline interpolation, an energy calibration via correlation[5] was used to calibrate the HED.

3.2.3 Time synchronization

The LED and HED have independent electronics and thereby different time information. To find events which could come from a Compton scattering

[4] A spline is a fitted polynomial between two points of a data set. The spline interpolation is the combination of such splines to realize a polynomial fit without oscillations between two points which can occur in high degree polynomial fits. See Späth (1995) for detailed information.

[5] See Maier and Limousin (2016) for an introduction to this method.

process[6], the time information of both detectors has to be synchronized. One possibility to perform a rough time synchronization is to use the mechanical shutter of the radioactive sources. Since the sources have different activities, a significant change in the hitrates of both detectors can be detected and analysed. With this method, the time can be synchronized up to an accuracy of $\Delta t \sim 10\,\mathrm{ms}$. For usual count rates of the CANDELA setup between 100 and 1000 counts per second, this accuracy is not good enough for a Compton event analysis because the two events from a Compton scattering process can not be identified. That is why fluorescence lines of the HED are used to increase the accuracy of the time synchronization. The LED events can be filtered for energies of the Cd-K_α fluorescence line $E^{\mathrm{Cd}}_{\mathrm{K}_\alpha} = 23.2\,\mathrm{keV}$. Those events were emitted from the HED which can be filtered for the most energetic photons of the CANDELA setup coming from the americium source with an energy of $E^{\mathrm{Am}} = 59.54\,\mathrm{keV}$ according to Table 1.1. With those fluorescence lines, a more accurate time synchronization of $\Delta t \sim 1\,\mathrm{ms}$ was done.

3.3 Analysis of Compton scattering events

To analyse the Compton scattered photons, the necessary information of the Compton events according to Table 3.1 listed in a fits file have to be collected.

Table 3.1: Data structure of the fits file containing Compton events. There are four columns for the LED and four columns for the HED with the pixel, energy and time information.

Detector	LED			
Column number	1	2	3	4
Content	Pixel x	Pixel y	Energy [eV]	Time [s]
Detector	HED			
Column number	5	6	7	8
Content	Pixel x	Pixel y	Energy [eV]	Time [s]

That means that after the energy calibration is done, the Compton events have to be filtered out of the data set of a measurement. Therefore, the time information of the data have to be considered. The events in the LED and HED arose from one Compton scattering process have to be

[6] A Compton scattering process contains one event in the LED and one event in the HED within a defined time interval which was set to $\Delta t_{\mathrm{Compton}} = 0.3\,\mathrm{ms}$.

detected at the same time[7]. The time interval in which both photons of one Compton event have to be detected was set to

$$\Delta t_{\text{Compton}} = 0.3\,\text{ms} \quad . \tag{3.17}$$

The presented measurement of Chapter 2 which was used for the Compton analysis with a total amount of $N_{\text{LED}} = 1.8 \times 10^6$ events for the LED and $N_{\text{HED}} = 3.2 \times 10^6$ events for the HED contained $N_{\text{Compton}} = 530$ Compton events which passed the defined filters. In Figure 3.2, the time information of the detected Compton events are shown. There are two time intervals with a duration of 4600 s and 4300 s without any Compton events. In those intervals, the time synchronization of the detectors could not be ensured and therefore no supposed Compton events were taken for the analysis. The smallest time gap between two Compton events was measured to be $t_{\text{min}} = 59\,\text{ms}$.

For a conclusive assignment of the LED and HED events which arose from one Compton scattering process, a filter for the energy was implemented. The analysis of Compton scattering events was limited for photons coming from the americium source with an energy of $E_{\text{Am}} = 59.54\,\text{keV}$. Therefore, the energy of the HED event has to be below this threshold and the total energy of the LED and the corresponding HED events has to be about this defined energy. To consider statistical fluctuations in the energy, Compton events with an total energy of

$$E_{\text{Compton}} = 59.74 \ldots 60.34\,\text{keV} \tag{3.18}$$

were chosen for the analysis. Therefore, the assignment of the Compton events should had be done correctly[8].

With the remaining $N_{\text{Compton}} = 530$ events, the reconstruction can be performed to trace back the origin of the initial photons. According to equation (3.8), the scattering angle Θ can be calculated by using the detected photon energies in the LED and the HED and their locations of interactions with the two detectors. Therewith, the respective ellipse of each Compton scattering event can be calculated. Overlapping those ellipses at the source plane $z = z_{\text{S}}$, all of them should cross in one point which is equal to the position of the source. For an unknown position of the source plane z_{S}, this overlap can be executed for different values of z.

[7]The time of $t_\gamma \approx 3 \times 10^{-11}\,\text{s}$ which is needed for the photon to travel the distance of 10 mm from the LED to the HED is negligible small compared to the accuracy of the time synchronization of $\Delta t \sim 1\,\text{ms}$.

[8]The case that a pair of photons get detected in the LED and HED and fulfill the requirements of a Compton event randomly can not be excluded completely. Without the implemented filter for the energy of the americium source, this case would had been even more probably.

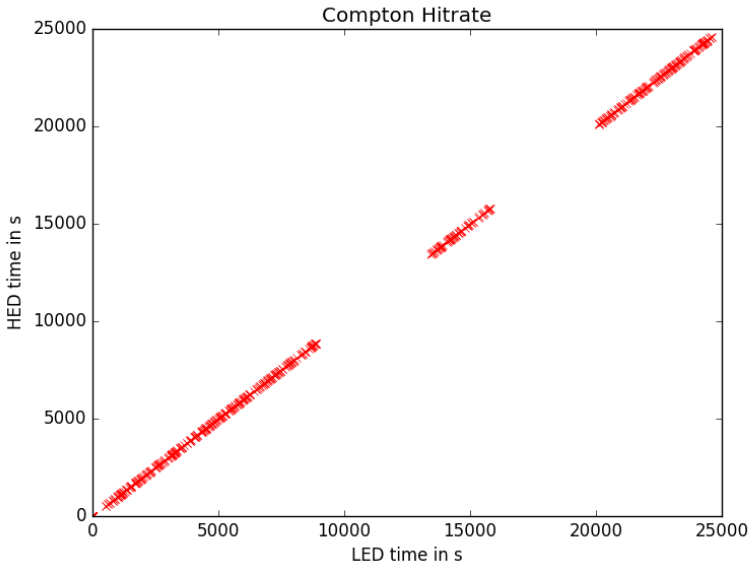

Figure 3.2: The time of the Compton events is plotted in this figure. The y-axis shows the time information of the LED and the x-axis shows the time information of the HED. There are two time intervals without any Compton events because in those intervals the time synchronization of the detectors could not be ensured.

For $z < z_S$ there are ellipses not crossing each other and the source position is outside of each ellipse. For $z > z_S$ all ellipses are crossing each other, but not at the same point. In this case, the source position is inside of each ellipse. Thereby, even a reconstruction of the source position in three dimensions is conceivable. In the following step, it is explained how the calculation of the ellipses can be performed.

As shown in Figure 3.1, the direction vector $\vec{r}$ pointing from the LED to the HED plane

$$\vec{r} = \begin{pmatrix} x_{\mathrm{LED}} - x_{\mathrm{HED}} \\ y_{\mathrm{LED}} - y_{\mathrm{HED}} \\ z_{\mathrm{LED}} - z_{\mathrm{HED}} \end{pmatrix} \tag{3.19}$$

can be calculated with the position of the events $(x_{\mathrm{LED}}, y_{\mathrm{LED}}, z_{\mathrm{LED}})$ and $(x_{\mathrm{HED}}, y_{\mathrm{HED}}, z_{\mathrm{HED}})$. By rotating this direction vector $\vec{r}$ with the angle Θ parallel to the LED plane and scaling the rotated vector to the source plane, one point of the ellipse (one possible origin of the respective photon) can be determined. The rotation axis $\vec{a}_i$ can be constructed for a defined amount

of total rotations N_{rot} with

$$\vec{a}_i = \begin{pmatrix} \cos\left(2\pi \frac{i}{N_{\mathrm{rot}}}\right) \\ \sin\left(2\pi \frac{i}{N_{\mathrm{rot}}}\right) \\ 0 \end{pmatrix} \tag{3.20}$$

where $i = 0 \ldots N_{\mathrm{rot}}$ is an integer. With the rotation axis $\vec{a}_i$ and the rotation angle Θ, a rotation matrix $R(\vec{a}_i, \Theta)$ can be calculated. For example Hanson (2011) explained that a rotation matrix $R(\vec{a}_i, \Theta)$ can be written as the exponential of an antisymmetric matrix

$$R(\vec{a}_i, \Theta) = \exp(\Theta \Lambda_{\vec{a}_i}) \tag{3.21}$$

with

$$\Lambda_{\vec{a}_i} = \begin{pmatrix} 0 & -a_{i3} & a_{i2} \\ a_{i3} & 0 & -a_{i1} \\ -a_{i2} & a_{i1} & 0 \end{pmatrix} \tag{3.22}$$

and $\vec{a}_i = (a_{i1}, a_{i2}, a_{i3})$. Since the exponential of a square matrix can be written as a Taylor series, the rotation matrix was calculated with an order of the Taylor series of 20

$$R(\vec{a}_i, \Theta) = \sum_{k=0}^{\infty} \frac{1}{k!} (\Theta \Lambda_{\vec{a}_i})^k \approx \sum_{k=0}^{20} \frac{1}{k!} (\Theta \Lambda_{\vec{a}_i})^k \quad . \tag{3.23}$$

With this matrix the rotation

$$\vec{r}_{\mathrm{rot}} = R(\vec{a}_i, \Theta) \cdot \vec{r} \tag{3.24}$$

and the scaling

$$\vec{r}_{\mathrm{scale}} = \vec{r}_{\mathrm{rot}} \frac{z_{\mathrm{S}}}{r_{\mathrm{rot},3}} \tag{3.25}$$

can be realized, where $r_{\mathrm{rot},3}$ is the third component of the vector $\vec{r}_{\mathrm{rot}}$. If this rotation is done for all values of i, the entire ellipse is calculated. The higher the value of N_{rot} is chosen, the preciser the ellipse can be determined. The superposition of all ellipses will indicate the most probably position of the source.

3.4 Results

Figure 3.3 to Figure 3.5 show the results of the implemented Compton analysis at three planes: $z = -130\,\text{mm}$, $z = -230\,\text{mm}$ and $z = -330\,\text{mm}$.

It can be seen that most of the ellipses are placed at negative values for y. This is the result of the eight pixel row measurement of the LED which was used for the analysis (Figure 2.2). Each detected Compton scattering event had a direction vector with a negative y component. The ellipses projected at positive y values had a high scattering angle Θ. According to the measured energies, the scattering angles were located at $\Theta = 14 \ldots 84\,°$.

It can be seen that the estimation of the position of the source in three dimensions can not be done without further optimization of the design. For the true value of the source plane $z = -230\,\text{mm}$, which is shown in Figure 3.4, all ellipses theoretically should overlap in one point for photons coming from the same point like source. This could not be reached because of the following uncertainties during the measurement.

- The limited resolution of the coordinates of an event in the LED and HED caused of a finite size of each pixel shifts the direction vector and thus the entire ellipse is displaced. For an estimation of the upper limit of this displacement, it can be assumed that the detected events

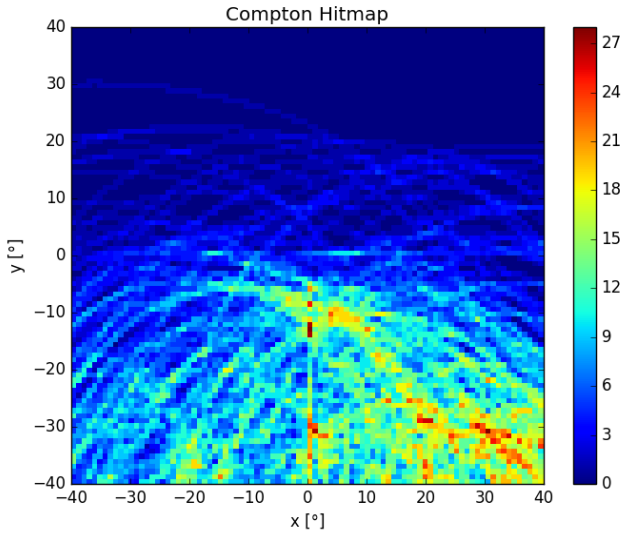

Figure 3.3: The hitmap of the Compton scattering events at $z = -130\,\text{mm}$ with a field of view of $40° \times 40°$ in the direction of the -z axis. The color coded values indicate the amount of ellipses crossing the respective coordinates.

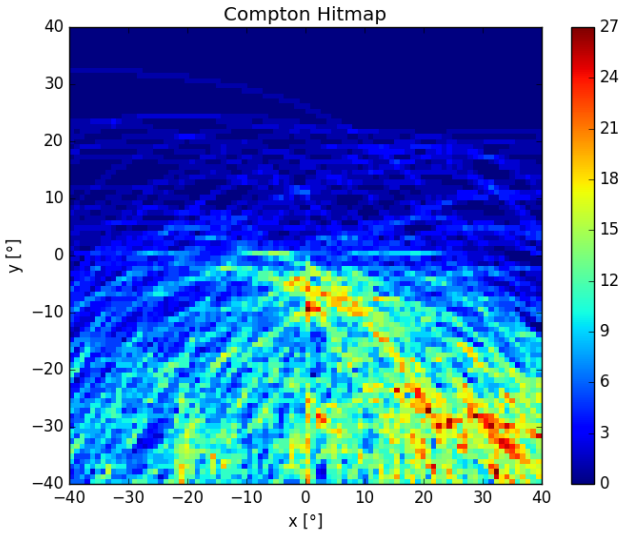

Figure 3.4: The hitmap of the Compton scattering events at $z = -230\,\mathrm{mm}$ with a field of view of $40\,^\circ \times 40\,^\circ$ in the direction of the -z axis. The color coded values indicate the amount of ellipses crossing the respective coordinates.

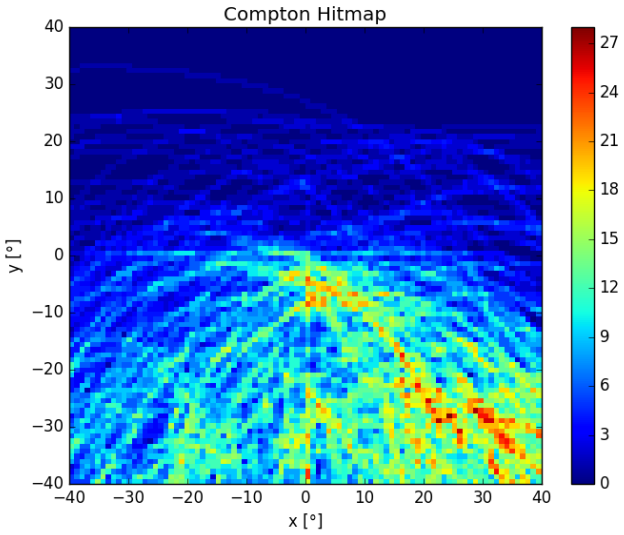

Figure 3.5: The hitmap of the Compton scattering events at $z = -330\,\mathrm{mm}$ with a field of view of $40\,^\circ \times 40\,^\circ$ in the direction of the -z axis. The color coded values indicate the amount of ellipses crossing the respective coordinates.

in the LED and the HED are shifted for a half pixel each in opposite directions. This would result in an upper limit of the displacement of $\Delta\alpha_{\text{Offset}} = 4.3\,^\circ$.

- According to Maier (2015), the uncertainties of the energy estimation of the LED is 2.8 % and for the HED 1.75 %[9]. Therewith, the scattering angle can not be calculated precisely and the corresponding ellipses are computed undersized or oversized. The uncertainty of the scattering angle $\Delta\Theta$ was calculated for each Compton scattering event according to Gaussian error propagation. The average of those uncertainties was estimated to be

$$\Delta\Theta = 0.9\,^\circ \quad . \tag{3.26}$$

  This value was chosen to be the resolution of the presented ellipses in Figure 3.3 to Figure 3.5.

- Two detected photons can fulfill the requirements coincidentally to be assigned as a Compton scattering event. The resulting ellipse can not contribute to the reconstruction of the source and is a source of background in the image.

The position of the source can not be clearly estimated by eye, but there are two areas $0\,^\circ < x < 10\,^\circ$, $-10\,^\circ < y < 0\,^\circ$ and $x > 15\,^\circ$, $y < -20\,^\circ$ with values up to 27 where a source could be located. The true position of the source was measured at the opened CANDELA setup to be at $(13.6\,^\circ, -17.4\,^\circ)$ and thereby outside of the estimated areas but in the correct corner of the plot. For a solid estimation of the source position in the image, a corresponding algorithm should be implemented in further work. In addition, the detectors of the CANDELA setup could be upgraded to have larger pixel matrices and a higher energy resolution which are important properties for a Compton camera. Furthermore, the software executing the analysis of the Compton scattering events should be extended to include the uncertainty of the energy determination for each ellipse. Thereby, the ellipses could also reflect a measure of the uncertainty of the direction vector $\vec{r}$ and the opening angle Θ that could be used in the illustrations as well as in the calculation of the source position.

The presented method to reconstruct the source position was chosen to illustrate the underlying theory and to get an estimation of the properties of the Compton scattering events. In further work this method should be discussed and replaced if needed.

[9] Those uncertainties were calculated at energies of 6 keV for the LED and 60 keV for the HED and can deviate for the energies of the Compton scattering events.

Chapter 4

Summary and conclusions

The work presented in this thesis is based on the stacked X-ray detector system CANDELA (**ca**dmium telluride and silico**n** **de**tector **la**boratory) developed at the IAAT. The CANDELA setup contains a low energy detector (LED) in front of a high energy detector (HED) with a very high quantum efficiency (close to 100 %) between 0.1 keV and 100 keV. This setup is equipped with radioactive materials as X-ray sources which can be selected by a mechanical shutter. The scientific data of both detectors are transmitted to a computer station where the data analysis can be performed.

This thesis can be separated into two parts: the implementation of the CASIMEO (**C**ANDELA **a**nalysis **s**oftware **im**aging **e**vents **o**nline) software and the analysis of Compton scattering events to trace back the position of an X-ray emitting source.

The CASIMEO software is able to process the incoming data of CANDELA and display them. The hitmap of the pixel matrix, a hitrate in units per frame and a hitrate in units per time as well as the PHA (pulse height amplitude) spectrum can be shown by the software for the transmitted data of the LED and the HED. The operator can decide whether those plots will be shown or not. Futhermore, it can be chosen if the software analyses the LED or HED data only or both successively. The CASIMEO software was explained and the results of two measurements were presented in Chapter 2.

A software to analyse Compton scattering events detected by CANDELA was implemented in the second part of this thesis. In Chapter 3, the physical background of a Compton scattering event is explained as well as the idea of a Compton camera which uses the information of Compton scattering events to trace back the origin of the initial photons. For this, the position of the events in the LED and HED has to be well known as well as the deposited energy in both detectors. For a measurement with

530 analysed Compton scattering events, the source position could not be estimated correctly by eye. In further work, the spatial and the energy resolution should be improved and in addition, an algorithm for the determination of the position of one or more sources should be realized.

The extension of a two dimensional to a three dimensional position determination should be continued. Such a Compton camera could be developed to a portable device. The real advantage of a Compton camera is to image X-rays without any focusing optics and thus strongly reduced complexity.

In astrophysics, a stacked spectrometer could be used as a Compton telescope. Since such a telescope should have a high energy resolution, the determination of the source position in two dimensions could be performed very well. A Compton telescope does only need a few detected Compton scattering events to do an analysis of the origin of the initial photons and can be operated parallel to a spectrometer. The disadvantage in such a usage is that the field of view of the telescope would have to be limited. Otherwise, the spectrometer could not distinguish between different sources. Nonetheless, scientific observations can be done with such a setup. Especially the search of gamma-ray bursts can be done very well with a Compton telescope first because of its large field of view.

Acknowledgements

I thank all the people who supported and advised me during my bachelor thesis. Especially I thank

- **Prof. Dott. Andrea Santangelo**
  for the possibility to write this thesis at the IAAT and his animated manner to give lectures which inspired me a lot.

- **Dr. Chris Tenzer**
  for the supervision and proofreading of my thesis. Additionally, for the fact that his office door is open for all kinds of questions and not least for his friendly way to teach.

- **Dr. Daniel Maier**
  for the execution of the measurement and the provision of the fits files which were used for the Compton analysis.

- **Thomas Schanz**
  for all the cycling tours to the canteen regardless of the weather and the conversations on those ways.

Furthermore, I thank my family and friends for their support during my studies and all the members of the IAAT group for the nice working atmosphere.

List of Figures

List of Tables

Bibliography

R. B. Firestone, C. M. Baglin, and S. Chu. *Table of isotopes*. Number 4. Wiley, 1999. ISBN 9780471356332.

P. Fornasini. *The Uncertainty in Physical Measurements: An Introduction to Data Analysis in the Physics Laboratory*. Springer New York, 2008. ISBN 9780387786506.

J. Hanson. Rotations in three, four, and five dimensions. *ArXiv e-prints*, Mar. 2011.

S. Herrmann, W. Buttler, R. Hartmann, N. Meidinger, M. Porro, and L. Strueder. CAMEX readout ASICs for pnCCDs. *IEEE Nuclear Science Symposium Conference Record*, Oct. 2008. doi: 10.1109/NSSMIC.2008.4774983.

Y. Ichinohe, Y. Uchida, S. Watanabe, I. Edahiro, K. Hayashi, T. Kawano, M. Ohno, M. Ohta, S. Takeda, Y. Fukazawa, M. Katsuragawa, K. Nakazawa, H. Odaka, H. Tajima, H. Takahashi, T. Takahashi, and T. Yuasa. The first demonstration of the concept of "narrow-FOV Si/CdTe semiconductor Compton camera". *Nuclear Instruments and Methods in Physics Research A*, 806:5–13, Jan. 2016. doi: 10.1016/j.nima.2015.09.081.

F. Jansen, D. Lumb, B. Altieri, J. Clavel, M. Ehle, C. Erd, C. Gabriel, M. Guainazzi, P. Gondoin, R. Much, R. Munoz, M. Santos, N. Schartel, D. Texier, and G. Vacanti. XMM-Newton observatory. I. The spacecraft and operations. *Astronomy & Astrophysics*, 365:L1–L6, Jan. 2001. doi: 10.1051/0004-6361:20000036.

P. Léna, D. Rouan, F. Lebrun, F. Mignard, and D. Pelat. *Observational astrophysics*. Springer, Berlin; Heidelberg, 3. edition, 2012. ISBN 978-3-642-21814-9.

M. S. Longair. *High Energy Astrophysics*. Cambridge University Press, 3. edition, 2012. ISBN 978-0-521-75618-1.

D. Maier. Development of a stacked detector system and its application as an X-ray polarimeter, 2015. Dissertation, Institute for Astronomy and Astrophysics, Eberhard Karls University Tübingen.

D. Maier and O. Limousin. Energy calibration via correlation. *Nuclear Instruments and Methods in Physics Research A*, A812:43–49, 2016. doi: 10.1016/j.nima.2015.11.149.

A. Meuris, O. Limousin, F. Lugiez, O. Gevin, C. Blondel, F. Pinsard, M. C. Vassal, F. Soufflet, and I. Le Mer. Caliste 64, a new CdTe micro-camera for hard X-ray spectro-imaging. *Nuclear Instruments and Methods in Physics Research A*, 610:154–157, Oct. 2009. doi: 10.1016/j.nima.2009.05.071.

R. Nadege, B. Didier, G. Olivier, and M. Pierre. Extensive testing of Schottky CdTe detectors for the ECLAIRs X-Gamma-ray Camera on board the SVOM mission. *ArXiv e-prints*, Mar. 2010.

V. Schoenfelder, H. Aarts, K. Bennett, H. de Boer, J. Clear, W. Collmar, A. Connors, A. Deerenberg, R. Diehl, A. von Dordrecht, J. W. den Herder, W. Hermsen, M. Kippen, L. Kuiper, G. Lichti, J. Lockwood, J. Macri, M. McConnell, D. Morris, R. Much, J. Ryan, G. Simpson, M. Snelling, G. Stacy, H. Steinle, A. Strong, B. N. Swanenburg, B. Taylor, C. de Vries, and C. Winkler. Instrument description and performance of the Imaging Gamma-Ray Telescope COMPTEL aboard the Compton Gamma-Ray Observatory. *The Astrophysical Journal Supplement Series*, 86:657–692, June 1993. doi: 10.1086/191794.

H. Späth. *One Dimensional Spline Interpolation Algorithms*. Ak Peters Series. Taylor & Francis, 1995. ISBN 9781568810164.

M. C. Weisskopf, B. Brinkman, C. Canizares, G. Garmire, S. Murray, and L. P. Van Speybroeck. An Overview of the Performance and Scientific Results from the Chandra X-Ray Observatory. *Publications of the Astronomical Society of the Pacific*, 114:1–24, Jan. 2002. doi: 10.1086/338108.

M. V. Zombeck. *Handbook of Space Astronomy and Astrophysics*. Cambridge University Press, 3. edition, 2007. ISBN 0-521-78242-2.